Proceedings World Geothermal Congress 2020
Reykjavik, Iceland, April 26 – May 2, 2020

Relationships between Lithology, Permeability, Clay Mineralogy, and Electrical Conductivity in Icelandic Altered Volcanic Rocks

Léa Lévy[1,2], Benoit Gibert[3], David Escobedo[3], Patricia Patrier[4], Bruno Lanson[5], Daniel Beaufort[4], Didier Loggia[3], Philippe A. Pezard[3], Nicolas Marino[3]

[1]ÍSOR, Iceland GeoSurvey, Grensásvegur 9, 108 Reykjavík, Iceland

lea@isor.is

[2] Aarhus University, Institute for Geoscience, Hydrogeophysics group, 8000 Aarhus, Denmark

[3] Laboratoire Géosciences Montpellier, Université de Montpellier, France

[4]IC2MP, CNRS-UMR 7285, Hydrasa, University of Poitiers, Bâtiment B35, 6 Rue Michel Brunet, TSA 51106, 86073 Poitiers Cedex 9, France

[5]Univ. Grenoble Alpes, Univ. Savoie Mont-Blanc, CNRS, IRD, IFSTTAR, ISTerre, F-38000 Grenoble, France

Keywords: permeability, clay minerals, electrical conductivity, alteration.

ABSTRACT

Based on a set of 94 core samples extracted from the Krafla volcano (Iceland), we study the influence of primary lithology and hydrothermal activity on permeability. We also study the sensitivity of electrical parameters, which can be measured from geophysical profiles, to permeability changes in these altered volcanic rocks.

We classify the samples into two main lithological types: hyaloclastite, including tuff and breccia, and lava, including vesicular and dense parts of lava flows as well as dykes. Scanning Electron Microscope (SEM), X-ray Diffraction (XRD) analyses allow identifying three main types of clay minerals: (i) tri-octahedral smectite (saponite), often occurring as replacement of glassy material in hyaloclastite samples, and sometimes replaced by corrensite/chlorite, (ii) chlorite/corrensite filling vesicles and other pore types of lava samples and (iii) illite/smectite mixed layers, kaolinite and aluminous smectite (montmorillonite) observed more locally, in samples relatively close to the surface. We show that the total quantity of secondary minerals is mostly controlled by the primary lithology and permeability.

The most permeable samples are welded breccia (in the hyaloclastite group) and fractured basalts (in the lava group). The least permeable samples are felsic viscous lava flows and basaltic dykes, in which little clay content is usually found and coincides with low porosity. Hyaloclastite rocks generally have permeability higher than 10^{-17} m^2 (10^{-2} mDa), regardless of alteration degree.

The abundance of secondary minerals (mainly smectite, corrensite, chlorite and zeolites) generally increases with gas permeability in altered samples, regardless of original lithology. However, the permeability measured by water is significantly lower than gas permeability, especially in smectite-rich samples. Such a discrepancy can be explained by the fact that, due to a swelling behavior, smectite minerals can easily clog micro-fractures in saturated conditions.

Regarding the sensitivity of electrical parameters to permeability changes in altered volcanic rocks, we observe that, at salinity higher than 40 g/L (5 S/m), the total conductivity is proportional to the permeability. At low salinity, it is proportional to the product of permeability and smectite content. As a consequence, fractured altered rocks containing swelling clay minerals can be very conductive although poorly permeable to water. The high electrical conductivity in low-permeability smectite-rich samples is attributed to conduction pathways through connected smectite particles, which seal the former fracture network.

Our results illustrate the double influence of permeability on the electrical conductivity of volcanic rocks: (i) direct influence of water permeability on conductivity, as observed at high salinity and (ii) influence of primary permeability ("geological" permeability, before the formation of secondary minerals) on the abundance of electrically conductive connected smectite. Although in-situ hydrothermal flows are also affected by regional features, which cannot be reproduced at laboratory scale, our results provide additional guidance for the interpretation of geo-electrical measurements, in terms of past and present day fluid flow.

1. INTRODUCTION

Permeability is a key parameter for the qualification of geothermal reservoirs of economic interest [e.g. *Gudmundsson et al.*, 2010]. Several factors control the large scale "geological" permeability in a geothermal reservoir and its evolution upon hydrothermal circulation [*Avellaneda and Torquato*, 1991; *Belghoul*, 2008; *Johnson and Schwartz*, 1989; *Pezard*, 1990]. One of the current challenges in geothermal exploration is to distinguish active and fossil sections of geothermal systems. Fossil sections usually correspond to clogging of the smaller scale permeable network due to the precipitation of secondary minerals [*Flóvenz et al.*, 2012; *Flóvenz and Saemundsson*, 1993]. As opposed to observations in fossil hydrothermal areas, *Patrier et al.* [1996] observe that, within fracture-controlled permeable horizons where boiling and mixing of fluids take place, great amounts of smectite or smectite-rich mixed-layers are formed, at temperatures exceeding the known thermodynamic range for smectite stability (up to 205°C). The vertical distribution of clay minerals (both in the illite-smectite and chlorite-smectite series) is in agreement with the temperature distribution in most of the low-permeable horizons of geothermal reservoirs, however. This pattern, observed at various high-temperature geothermal fields such as in El-Salvador, Japan, Greece and Iceland [*Beaufort et al.*, 1997; *Bril et al.*, 1996; *Escobedo et al.*, 2018] suggest that the presence of smectite, outside the shallow clay cap, is a good indicator of recent active hydrothermal circulations.

Mapping the underground distribution of smectite in low-salinity geothermal systems, and thus locating recent up-flow zones, is possible thanks to electromagnetic and geo-electrical methods, although the resolution of these surface measurements still needs to be improved [*Lévy*, 2019; *Lévy et al.*, 2018; *Lévy et al.*, 2019b]. One limit to this approach is that smectite may have adverse effect on the originally high permeability allowing its formation: the swelling properties of smectite may decrease significantly the final permeability of the system.

Therefore, an improved description of the causality chain between lithology, alteration and permeability and, in particular, of the adverse effect of alteration mineralogy on permeability would help simulate the changes of fluid and heat transport due to secondary minerals precipitation in geothermal reservoirs, as well as in subduction zones [*Hyndman et al.*, 1997] and at major faults [*Chester et al.*, 2013]. More generally, a better understanding of the permeability of volcanic material is needed to predict explosive eruptions and flank collapses at volcanoes [*Heap et al.*, 2018].

The goal of this study is to investigate the interaction between transport properties (permeability, electrical conductivity), lithology and alteration mineralogy from hydrothermal activity (type and amount of secondary minerals).

2. MATERIALS AND METHODS

2.1 Samples

A total of 94 volcanic samples are used in this study. All samples are from the Krafla high-temperature geothermal field, where cores are available from four boreholes, down to 700 m (Figure 1). The Krafla field, where a geothermal powerplant has been in operation since 1977, is located within the caldera of the Krafla central volcano [*Sigmundsson*, 2006] in North-East Iceland. The texture of the samples varies from fully glassy basalt to highly crystalline basalt. The abundance of secondary minerals varies from 0 to 90 %.

2.2 Mineralogy

Five methods are used to characterize the mineralogy of the samples: Cation Exchange Capacity (CEC), powder X-ray Diffraction (XRD), XRD on oriented mounts of fine fractions (< 2 µm), Scanning Electron Microscope (SEM) and optical microscopy on thin sections.

The lithology of samples is determined from SEM and optical microscope observations, as well as naked-eye observations of the cores in their geological context (core boxes). Samples are first classified into five groups: hyaloclastite, tuffs and breccia, vesicular lava, crystalline basalt (e.g. central lava flow), dykes. A simplified lithological classification is used in our analysis: (i) glass-rich volcanic material, including hyaloclastite, tuff and breccia, referred to as “hyaloclastite” and (ii) crystalline volcanic rocks, including vesicular lava, central lava flows and dykes, referred to as “lava” (see Table 1 in Appendix).

Rietveld refinements of XRD patterns on whole rock powder samples allow quantitative (crystalline) phase analysis. The total percentage of alteration, presented in Table 1, is calculated based on the sum of the percentages of secondary minerals (mostly clay minerals, zeolites, quartz, calcite and pyrite) resulting from the Rietveld refinement. In addition, CEC measurements provide a more accurate determination of the smectite volume fraction, according to the following equation:

$$Smec_{vol.\%} = \frac{CEC}{CEC_0}\frac{\rho_{dry}}{\rho_{smec}}, \quad (1)$$

where CEC and CEC_0 are the CEC of the sample and of pure smectite in meq/100g, respectively, and ρ_{dry} and ρ_{smec} are the density of the dry sample and of smectite in g/cm^3, respectively. The value of $CEC_0 = 91$ meq/100g is used, according to results by [*Lévy et al.*, 2019a; *Lévy et al.*, 2018].

XRD measurements on fine fractions provide details about the crystalline structure of clay minerals. Analyses have been carried out on Na-saturated samples (air-dried), as well as on ethylene-glycol-saturated samples.

SEM observations combined with Energy Dispersive Spectroscopy (EDS) are used to validate the clay minerals chemical composition. The following clay minerals are found: saponite (tri-octahedral smectite), corrensite (mixed-layer smectite/chlorite), chlorite, montmorillonite (di-octahedral smectite), kaolinite and mixed-layer illite-smectite.

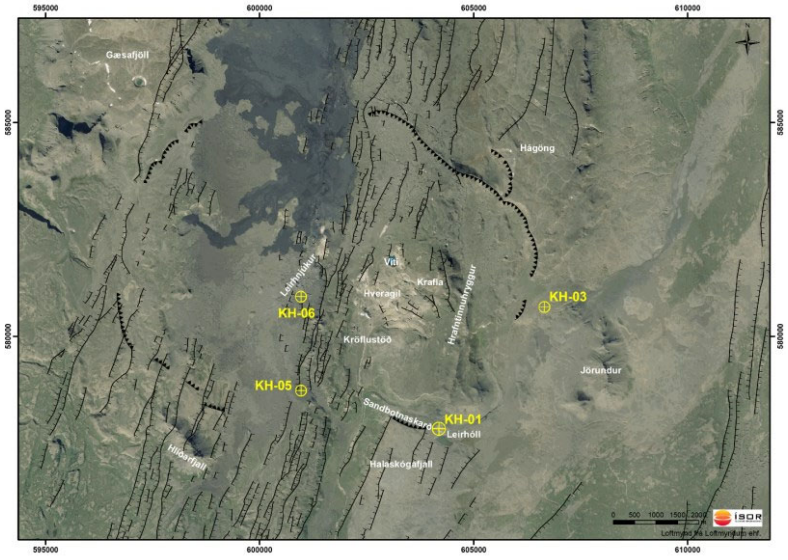

Figure 1. Aerial map of the Krafla volcano. The caldera rims and N-S trending fissure swarms are indicated with black triangles and lines, respectively. The four cored boreholes used in this study are indicated in yellow (KH-01, KH-03, KH-05 and 06).

2.3 Petrophysics

The porosity and density are determined on saturated core samples using the 'Triple Weighting' method: the plug mass is first measured on dry samples (dried at 60°C in an oven for 48 hr), then measured on saturated samples, and finally measured in immersed conditions. The plugs are saturated with low-salinity degassed water (water conductivity of about 100 µS/cm) after evacuating air-filled pores in a vacuum chamber.

Permeability is measured with gas (argon Ar) for 55 samples and with water for 49 samples. Permeability is determined using a stationary method on cylindrical samples maintained at a confining pressure ranging from 4 to 5 MPa. On one end of the sample, the pore pressure is systematically kept constant and equal to 0.1 MPa (atmospheric pressure), while at the second end a pore pressure ranging from 0.5 to 3 MPa is kept constant, thus allowing a constant pressure gradient Δp. In Ar-permeability measurements, the volumetric flow rate q is measured by commercial flow-meters. In water-permeability measurements, a servo-controlled pump kept the pore pressure constant and the flow rate is determined using the measured piston displacement. Permeability is calculated using Darcy's law. In the case of Ar-permeability, Darcy's law is modified to take into account fluid compressibility [*Heap et al.*, 2018]. The Klinkenberg effect is also quantified by performing successive measurements at different pore pressure gradients. For samples with permeability lower than 10^{-19} m^2 (10^{-4} mDa), a conventional pulse decay method is used [e.g.*Brace et al.*, 1968].

Electrical conductivity is measured on samples saturated with water at different salinities, using a Solartron 1260 impedance-meter (alternative source at variable frequency) and a two-electrode set-up, where the sample is sandwiched between two metallic electrodes acting as current and voltage electrodes. Only results measured at 1 kHz and at the two extreme salinities (0.3 g/L and 90 g/L corresponding to 0.05 S/m and 11 S/m, respectively) are presented her.

An apparent formation factor is determined at each salinity, by the following equation:

$$\frac{1}{F_{app}} = \frac{\sigma_0}{\sigma_w}, \quad (2)$$

where F_{app} is the apparent formation factor (dimensionless), σ_0 is the electrical conductivity of the sample and σ_w is the electrical conductivity of the pore water (S/m). Then, the increase of F_{app} with salinity is fitted with the function presented in the following equation, as suggested by *Weller et al.* [2013],

$$F_{app} = \frac{FF\sigma_w}{a+\sigma_w}, \quad (3)$$

where FF and a are the true formation factor and a free parameter (in S/m), respectively. This equation yields a formation factor F relatively close to a linear fit, corresponding to Archie's law [*Archie*, 1942].

3. RESULTS

3.1 Lithology and fractures control permeability and quantity of secondary minerals

3.1.1 Influence of lithology on permeability and density

Gas (argon) permeability is always higher than water permeability (**Error! Reference source not found.**2). The permeability of hyaloclastite samples reaches higher values and covers a narrower range the permeability of lava samples, for both gas and water measurements. The ranges for hyaloclastite are 10^{-2}-10^{1} mDa and 10^{-4}-10^{0} mDa for gas and water, respectively, while the ranges for lava are 10^{-5}-10^{0} mDa and $<10^{-6}$-10^{0} mDa, respectively (**Error! Reference source not found.**3). The higher variability of permeability observed for the lava group, compared to that of the hyaloclastite group, can be explained by a higher dependency on the extent of fracturation for crystalline samples. The water/gas permeability ratio seems to be independent from lithology.

The grain density of hyaloclastite is generally lower than that of lavas, but also covers a wider range (Figure 4a). The grain density seems to be primarily influenced by lithology, with lavas and in particular intrusions being denser than glassy material. Six lava samples have a grain density higher than 3.0 g/cm^3. In general, an increased percentage of secondary minerals (clay minerals and zeolites in particular) corresponds to a decrease of the grain density, for both hyaloclastites and lavas. The percentage of secondary minerals itself can be partially influenced by lithology because volcanic glass may alter more easily than lava (Figure 4). Ten lava samples have a percentage of alteration lower than 10%.

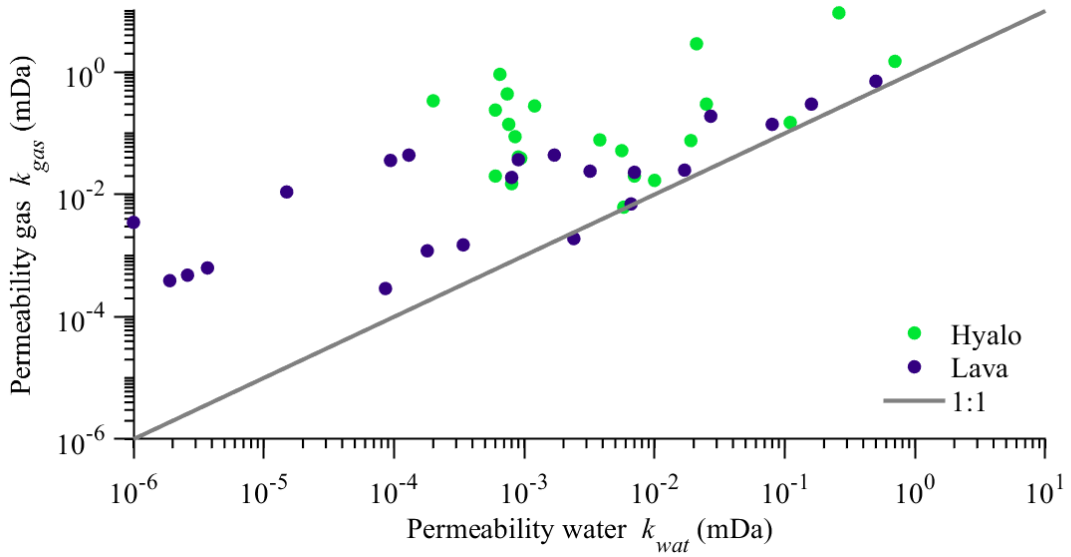

Figure 2. Gas versus water permeability. Blue and green colors are meant to identify the lithological groups. The grey line corresponds to the function k_gas=k_wat.

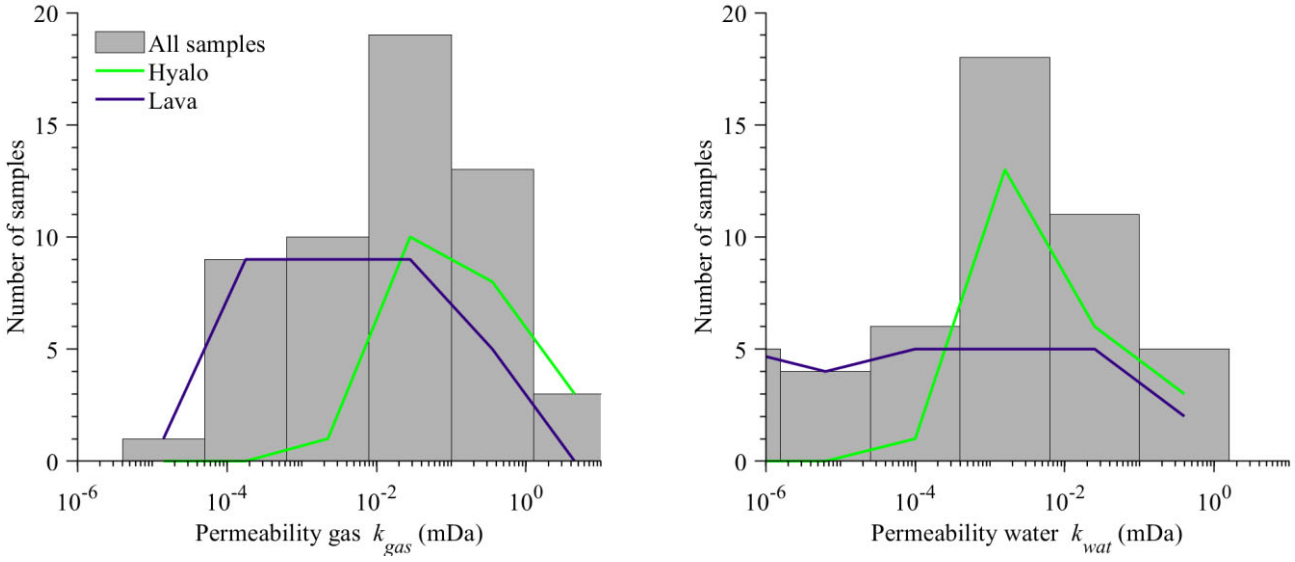

Figure 3. Distribution of permeability measured with gas and water for all samples. The black and blue lines represent the number of samples in each bin for hyaloclastite and lava, respectively.

3.1.2 Relation between permeability, density and amount of secondary minerals

We observe that an increased gas permeability corresponds to a general increase of the quantity of secondary minerals (Figure 4b), with hyaloclastite samples generally more altered than lavas. The correlation between alteration quantity and permeability is lost when looking at water permeability (Appendix A). This indicates that water permeability might be significantly affected by clogging of the permeable network upon alteration than gas permeability already is. The presence of secondary minerals is also associated to a reduced average grain density (Figure 4a).

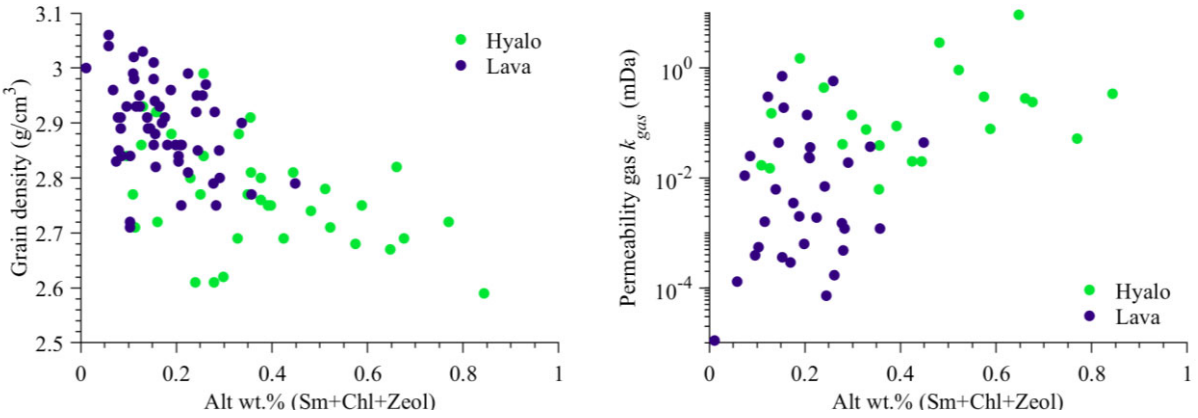

Figure 4. Percentage of secondary minerals (smectite, chlorite, zeolites) versus (a) grain density and (b) gas permeability.

3.1.3 Relation between lithology and the nature of clay minerals

XRD analyses on oriented mount allow identifying three types of clay minerals. The two main types are illustrated in Figure 5: (i) tri-octahedral smectite (saponite) and (ii) corrensite/chlorite. We see in particular that, in chlorite/smectite mixed-layer clays (e.g. in samples L82 and L103), little swelling occurs upon saturation with ethylene-glycol, as opposed to pure saponite (samples L96 and L119). The third type of clay minerals, corresponding to mixed-layer illite-smectite (I/S) and di-octahedral smectite (montmorillonite), is only found locally, in highly altered zones where a complete replacement of primary minerals has taken place. More details can be found in *Escobedo* [2018].

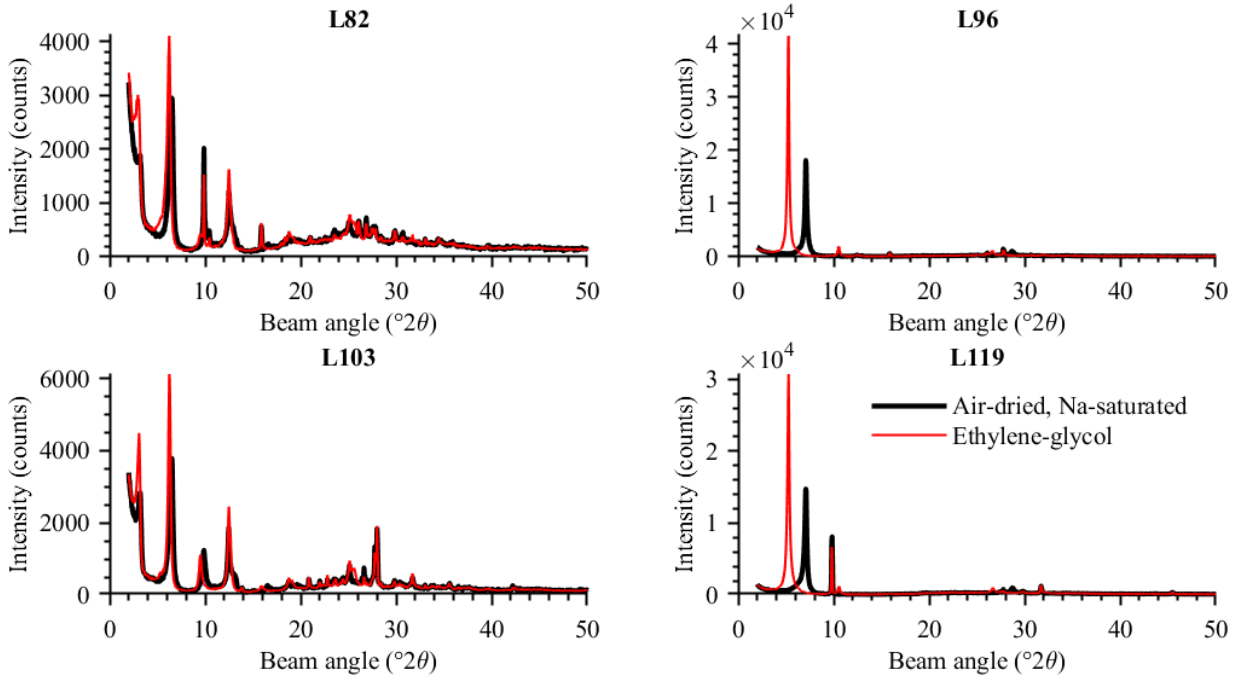

Figure 5. XRD scans on oriented mounts of fine fractions (< 2µm) for four samples. The black and red colors correspond to Na-saturated (air-dried) and ethylene-gylcol-saturated samples. Samples L82 and L103 (lavas, from borehole KH-06) show typical chlorite/corrensite patterns, while L96 and L119 (hyaloclastites, from boreholes KH-03 and KH-06, respectively) show typical saponite patterns.

Saponite is most abundant in hyaloclastite samples, while the combination corrensite/chlorite is dominant in lavas (Figure 6). However, in one borehole (KH-05) where high-temperature alteration minerals (epidote, actinolite, wairakite) are abundant, chlorite is the dominant type of clay mineral everywhere, even in hyaloclastites. All hyaloclastite samples having a chlorite/smectite ratio higher than one come from borehole KH-05. In this borehole, chlorite and corrensite may have progressively replaced saponite,originally formed as glass replacement, whereas, in other boreholes, chlorite and corrensite may have precipitated directly in the porosity.

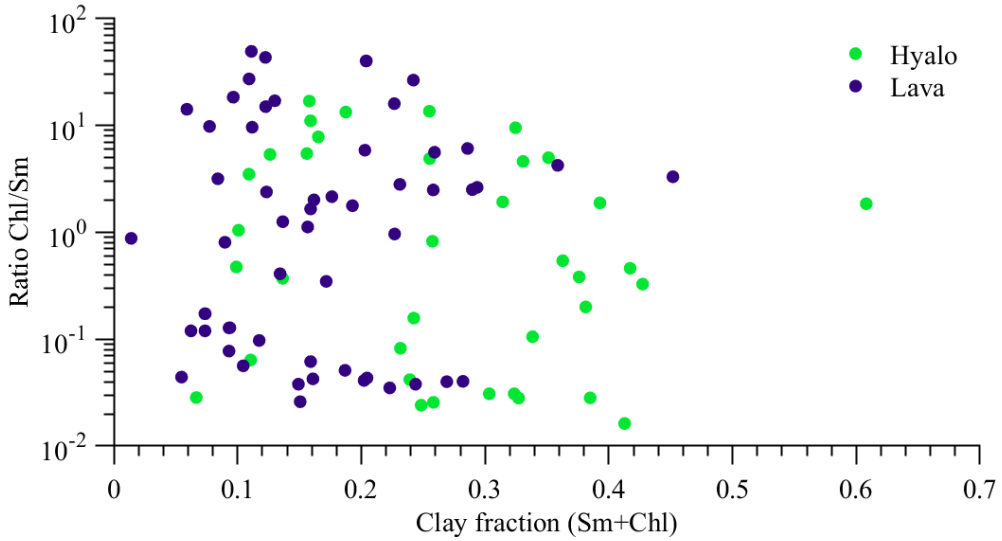

Figure 6. Ratio chlorite/smectite versus total clay fraction (more exactly the sum of smectite and chlorite). The chlorite fraction is that quantified by Rietveld refinements of XRD patterns, while the smectite fraction is calculated using the CEC and equation 1.

3.2 Water to gas permeability ratio controlled by smectite to pore volume ratio.

The water/gas permeability ratio appears influenced by the type of secondary minerals, in particular by the smectite content (

Figure 7). We introduce the parameter Q_v used by [*Waxman and Smits*, 1968], e.g., to describe the electrical conductivity of shaly sands.

$$Q_v = \rho_g CEC \frac{1-\phi}{\phi}, \quad (4)$$

Where ρ_g, CEC and ϕ are the grain density (g/cm3), Cation Exchange Capacity (meq/100g) and porosity (dimensionless), respectively. After normalization (presented in equation 5), $Q_{v,n}$ corresponds to the ratio between smectite volume and total volume of connected pores (including connected vesicles, micro-fractures and joints), as presented by [*Lévy et al.*, 2018].

$$Q_{v,n} = \frac{Q_v}{CEC_0 \rho_{smec}}, \quad (5)$$

Where CEC_0 and ρ_{smec} are the CEC of pure smectite (91 meq/100g for these rocks) and the density of smectite (2.3 g/cm^3).

The ratio $Q_{v,n}$ seems to control the decrease from gas to water permeability. Beyond a threshold of 30% (smectite/pores), the water/gas permeability ratio linearly decreases from one to 10^{-4} with increasing ratio smectite/pores (reaching up to 300%). The ratio $Q_{v,n}$ can exceed 100% because the volume of smectite formed upon hydrothermal reactions is not limited by the volume of pores. A minimum porosity is needed to allow hydrothermal fluid to circulate but then smectite also replaces glass or plagioclases, in addition to fill-in the porosity. All samples with a water/gas permeability ratio equal to unity have more chlorite than smectite. No clear influence of the lithological type on the water to gas permeability ratio is observed.

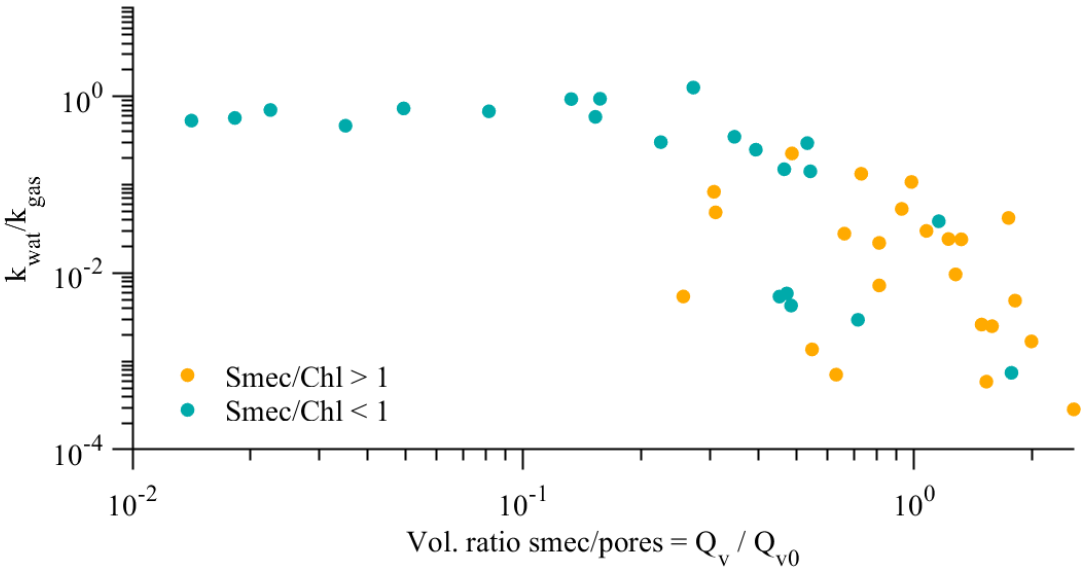

Figure 7. Water to gas permeability ratio versus smectite to pore volume ratio. The two colors separate samples with more chlorite than smectite and samples with more smectite than chlorite.

3.3 Electrical conductivity at high salinity controlled by water permeability

Electrical conductivity of samples saturated with high-salinity brine (water conductivity of 11 S/m) is mostly correlated to the water permeability, with a weak power law (exponent 0.23, Figure 7). This indicates that at this salinity, both properties are similarly influenced by the geometry of the pore space. This relationship is expected because (i) the electrical conductivity at high-salinity is mostly influenced by the formation factor [*Archie*, 1942; *Avellaneda and Torquato*, 1991] and (ii) the formation factor and the water permeability are related by a power law [*Gueguen and Dienes*, 1989], as illustrated in Figure 9. The correlation coefficient R^2 is higher with water permeability than with gas permeability. At high salinity, hyaloclastite samples are generally more conductive than lavas.

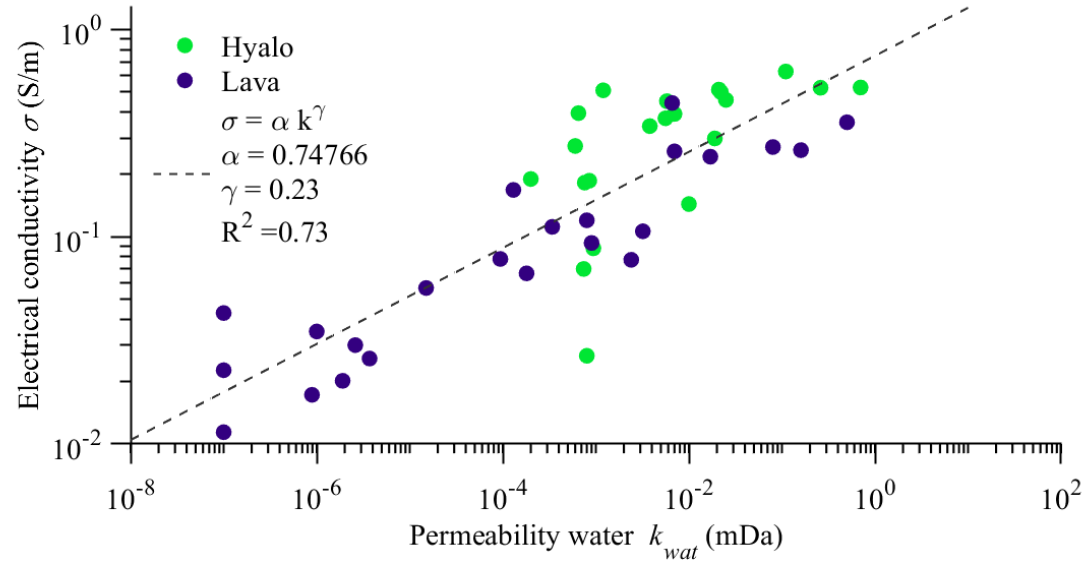

Figure 8. Electrical conductivity, measured on samples saturated with high-salinity brine (fluid conductivity 11 S/m), versus water permeability.

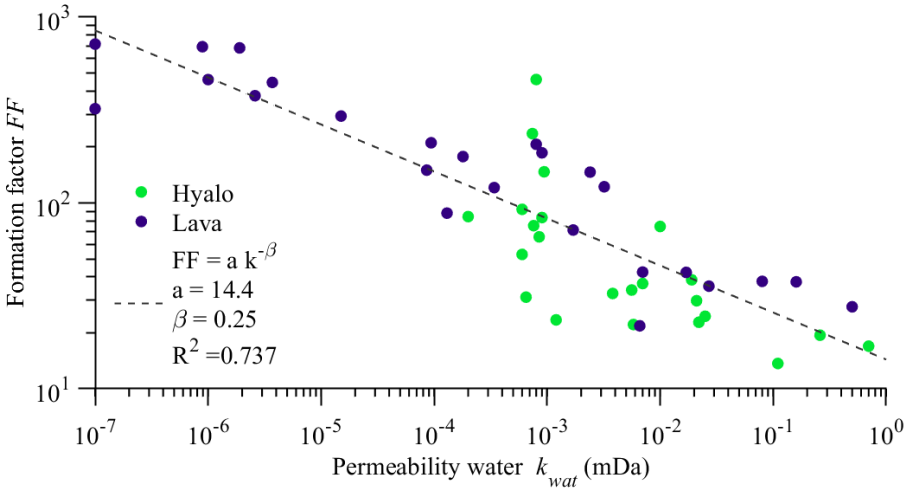

Figure 9. Formation factor versus water permeability. The formation factor (FF) is determined based on electrical conductivity measurements over a wide range of salinity.

3.4 Electrical conductivity at low salinity controlled by water permeability and smectite volume

When volcanic rocks are saturated with low-salinity water – as it is the case in most geothermal fields such as Krafla – not only the water permeability (or formation factor) influences the electrical conductivity of these rocks; the smectite volume also has a key influence. A linear relationship is found between the "low-salinity" electrical conductivity and the smectite volume to formation factor ratio (Figure 10). We use this ratio in order to combine in a single trend samples with significant smectite volume (where conductivity is mostly controlled by the smectite content) and samples with negligible smectite volume (where conductivity is mostly controlled by formation factor). The most conductive samples at low salinity are hyaloclastite but a series of hyaloclastite samples have conductivity as low as lavas: these samples contain chlorite but no smectite.

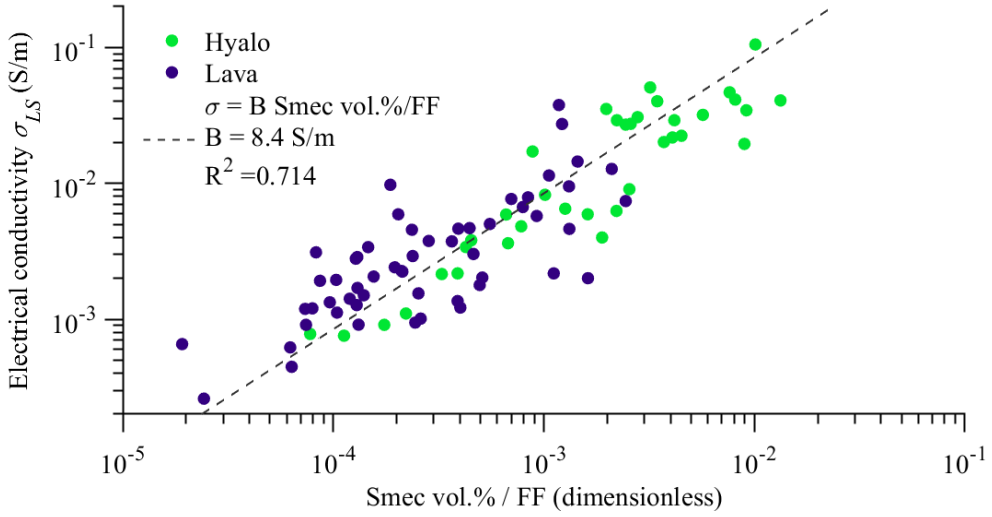

Figure 10. Electrical conductivity measured on sample saturated with low-salinity water (0.03-0.07 S/m) versus smectite volume fraction to formation factor ratio.

4. DISCUSSION

The primary permeability, before alteration processes take place, determines the flow rates that have been able to go through the rock. This permeability can be mitigated upon alteration, by re-distribution of the porosity. The extent of alteration itself depends on the flow rates that go through the rock, but also on the ability of the rock to be altered, with glass (abundant in hyaloclastite) being more rapidly altered than crystalline rocks (such as dyke or lava flows). Therefore, the gas permeability, measured in laboratory, depends on the primary permeability but the difference between primary and gas permeability may depend on the lithology.

We observe that gas permeability is in average higher for hyaloclastite than for lavas, while hyaloclastite samples are generally more altered than lavas (Figure 4b). Since the gas permeability gives a lower limit of the primary permeability and that the difference primary-gas permeability is likely to be higher in hyaloclastite (more altered), our observations suggest that the primary permeability of hyaloclastite is generally higher than the primary permeability of lavas. Lavas also cover a wider range of gas permeability than

hyaloclastites. This could be the effect of fracturing to variable extent, which would be the controlling factor for primary permeability in lavas, even at the laboratory scale. Estimating the fracture density would help to confirm this interpretation.

We see that lava samples with water permeability higher than 10^{-3} mDa have mostly chlorite as clay minerals (Table 1). This suggests that a high gas permeability favors the apparition of secondary minerals, and that as long as smectite represents only a small fraction of these secondary minerals, the permeability (both gas and water) is not retroactively affected. On the other hand, if smectite represents a large part of the secondary minerals, the permeable network may be clogged when samples are water-saturated, due to swelling of smectite in the presence of water.

Electrical conductivity at high salinity is mostly influenced by the water permeability (Figure 8) but we suggest that it is also indirectly affected by the smectite content, since the water permeability tends to decrease with the smectite content. Electrical conductivity at low salinity is influenced by both smectite content and water permeability (Figure 9 and Figure 10). At low salinity, such as in the Krafla geothermal system, even rocks with low water permeability ($<10^{-3}$ mDa) can be very conductive. This is interpreted as the effect of electrical conduction through connected smectite pathways in the solid, as suggested by *Lévy et al.* [2018].

These observations and interpretations are summarized with a schematic representation in Figure 11.

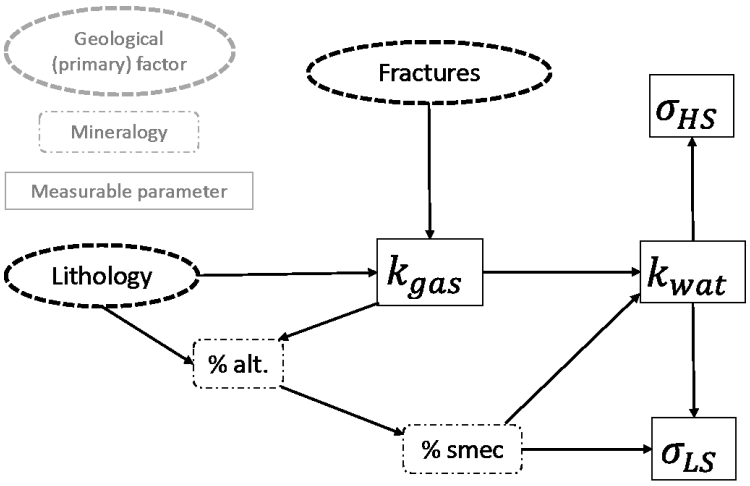

Figure 11. Schematic representation of the influence of geological factors on measurable petrophysical parameters

5. CONCLUSIONS

The lithology, clay mineralogy, grain density, permeability with gas and water, as well as electrical conductivity at low and high salinity of a large sample set are analyzed, in order to better understand how rock parameters influence each other in geothermal fields.

Hyaloclastite generally have higher gas permeability and alteration content than lavas. The water/gas permeability ratio is independent from lithology but controlled by the nature of secondary minerals, in particular by smectite content. The ratio smectite volume to total volume of connected pores ratio (including connected vesicles, micro-fractures and joints) seems to control the decrease from gas to water permeability. Beyond a threshold of 30% (smectite/pores), the water/gas permeability ratio linearly decreases from one to 10^{-4} with increasing ratio smectite/pores (reaching up to 300%). All samples with a water/gas permeability ratio equal to unity have more chlorite than smectite.

As expected, water permeability is more closely related to the electrical properties of water-saturated volcanic rocks than gas permeability. Electrical conductivity of high-salinity brine saturated samples (water conductivity of 11 S/m) is mostly influenced by water permeability, with a weak power law (exponent 0.25). Similarly, the electrical formation factor is inversely correlated to water permeability with a weak power law (exponent -0.25). These two relationships are consistent with the fact that electrical conductivity of brine saturated rocks is inversely proportional to the formation factor.

When volcanic rocks are saturated with low-salinity water – as for most geothermal fields such as Krafla – not only water permeability (or formation factor) influences the electrical conductivity of these rock, but the smectite volume also plays a key role. A linear relationship is found between the "low-salinity" electrical conductivity and the smectite volume to formation factor ratio.

In addition to smectite content and water permeability, primary lithology appears also to have an influence on electrical conductivity. Hyaloclastite samples generally have higher electrical conductivity than crystalline samples, both at low and high salinity, but hyaloclastite samples containing more chlorite than smectite have electrical conductivity in the same range as crystalline samples, especially at low salinity.

5. ACKNOWLEDGMENTS

The authors thanks the power company Landsvirkjun for providing access to core samples several times in very good conditions. L.L. thanks ÍSOR for the help for handling the samples and understanding their mineralogy, and more particularly Albert Þorbergsson for the creation of adequate maps of Krafla. Christophe Nevado and Doriane Delmas are warmly thanked for the preparation of high-

quality thin sections. Nathaniel Findling is thanked for his help with XRD analyses and interpretation. This work was supported by a PhD grant from Paris Sciences et Lettres to Léa Lévy and the IMAGE FP7 EC and GEMex H2020 projects (grant agreements 608553 and 727550), as well as by a CNRS-INSU grant (TelluS program) attributed to the project AGERG. Fundings for travelling were provided by the PHC program JulesVerne, granted to Ecole Normale Supérieure and University of Iceland, by the Icelandic Centre for Research (Rannis) and the French Ministries of Foreign Affairs and International Development and of Education, Teaching and Research.

REFERENCES

Archie, G. E. (1942), The electrical resistivity log as an aid in determining some reservoir characteristics, Transactions of the AIME, 146(01), 54-62.

Avellaneda, M., and S. Torquato (1991), Rigorous link between fluid permeability, electrical conductivity, and relaxation times for transport in porous media, Physics of Fluids A: Fluid Dynamics, 3(11), 2529-2540.

Beaufort, D., P. Papapanagiotou, P. Patrier, K. Fujimoto, and K. Kasai (1997), High-temperature smectites in active geothermal systems, paper presented at Proceedings 8th Water-Rock Interaction Symposium, Vladivostok, 1995.

Belghoul, A. (2008), Caractérisation pétrophysique et hydrodynamique du socle cristallin, Université de Montpellier.

Brace, W. F., J. B. Walsh, and W. T. Frangos (1968), Permeability of granite under high pressure, Journal of Geophysical research, 73(6), 2225-2236.

Bril, H., P. Papapanagiotou, P. Patrier, J.-F. Lenain, and D. Beaufort (1996), Fluid-rock interaction in the geothermal field of Chipilapa (El Salvador): contribution of fluid-inclusion data, European Journal of Mineralogy, 515-532.

Chester, F. M., et al. (2013), Structure and composition of the plate-boundary slip zone for the 2011 Tohoku-Oki earthquake, Science, 342(6163), 1208-1211.

Escobedo, D. (2018), Study of hydrothermal alteration and petrophysical properties of well KH6, Krafla geothermal field, NE Iceland, University of Montpellier.

Escobedo, D., P. Patrier, B. Gibert, L. Lévy, B. Lanson, D. Beaufort, and J. Caillaud (2018), Clay minerals distribution and petrophysical properties at borehole KH6, Krafla, Iceland, edited.

Flóvenz, Ó. G., G. P. Hersir, K. Sæmundsson, H. Ármannsson, and T. Friðriksson (2012), 7.03 - Geothermal Energy Exploration Techniques, in Comprehensive Renewable Energy, edited by A. Sayigh, pp. 51-95, Elsevier.

Flóvenz, Ó. G., and K. Saemundsson (1993), Heat flow and geothermal processes in Iceland, Tectonophysics, 225(1-2), 123-138.

Gudmundsson, Á., A. K. Mortensen, A. Hjartarson, R. Karlsdóttir, and H. Ármannsson (2010), Exploration and utilization of the Namafjall high temperature area in North Iceland, paper presented at World Geothermal Congress, 2010.

Gueguen, Y., and J. Dienes (1989), Transport properties of rocks from statistics and percolation, Mathematical geology, 21(1), 1-13.

Heap, M. J., T. Reuschlé, J. I. Farquharson, and P. Baud (2018), Permeability of volcanic rocks to gas and water, Journal of Volcanology and Geothermal Research, 354, 29-38.

Hyndman, R. D., M. Yamano, and D. A. Oleskevich (1997), The seismogenic zone of subduction thrust faults, Island Arc, 6(3), 244-260.

Johnson, D. L., and L. M. Schwartz (1989), Unified theory of geometrical effects in transport properties of porous media, paper presented at SPWLA 30th Annual Logging Symposium, Society of Petrophysicists and Well-Log Analysts, Denver, Colorado, 1989.

Lévy, L. (2019), Electrical properties of hydrothermally altered rocks: observations and interpretations based on laboratory, field and borehole studies at Krafla volcano, Iceland, Ecole Normale Supérieure and University of Iceland.

Lévy, L., T. Fridriksson, N. Findling, B. Lanson, B. Fraisse, and B. Gibert (2019a), Smectite quantification in hydrothermally altered volcanic rocks, submitted to Geothermics.

Lévy, L., B. Gibert, F. Sigmundsson, Ó. G. Flóvenz, G. P. Hersir, P. Briole, and P. A. Pezard (2018), The role of smectites in the electrical conductivity of active hydrothermal systems: electrical properties of core samples from Krafla volcano, Iceland, Geophysical Journal International, 215(3), 1558-1582.

Lévy, L., P. K. Maurya, S. Byrdina, J. Vandemeulebrouck, F. Sigmundsson, K. Arnason, and e. al. (2019b), Electrical Resistivity Tomography and Time-Domain Induced Polarization field investigations of geothermal areas at Krafla, Iceland: comparison to borehole and laboratory frequency-domain electrical observations, Geophysical Journal International.

Patrier, P., P. Papapanagiotou, D. Beaufort, H. Traineau, H. Bril, and J. Rojas (1996), Role of permeability versus temperature in the distribution of the fine (≤ 0.2 μ m) clay fraction in the Chipilapa geothermal system (El Salvador, Central America), Journal of Volcanology and Geothermal Research, 72(1), 101-120.

Pezard, P. A. (1990), Electrical properties of mid-ocean ridge basalt and implications for the structure of the upper oceanic crust in Hole 504B, Journal of Geophysical Research, 95(B6), 9237-9237.

Sigmundsson, F. (2006), Iceland geodynamics: crustal deformation and divergent plate tectonics, Springer Science & Business Media.

Waxman, M. H., and L. J. M. Smits (1968), Electrical conductivities in oil-bearing shaly sands, Soc. Pet. Eng. J., 8, 107-122.

Weller, A., L. Slater, and S. Nordsiek (2013), On the relationship between induced polarization and surface conductivity: Implications for petrophysical interpretation of electrical measurements, Geophysics, 78(5), D315-D325.

APPENDIX A. SECONDARY MINERALS AND PERMEABILITY

In Figure A.1. we present results of secondary minerals quantification versus water permeability, to illustrate the absence of correlation, as opposed to Figure 4b, where gas permeability is shown.

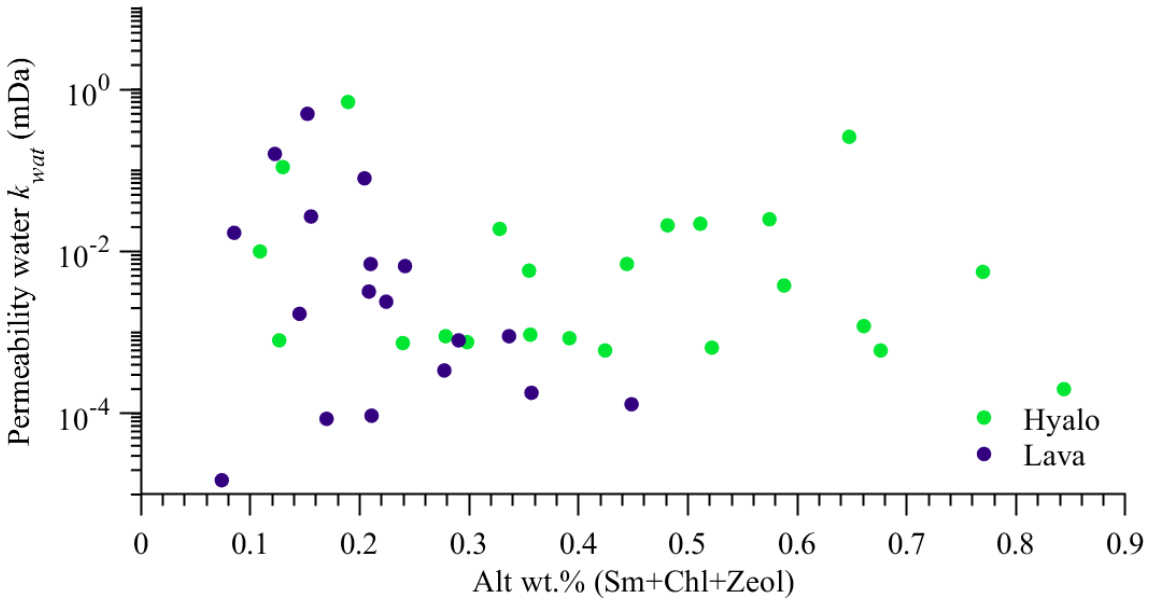

Figure A.1. Water permeability versus weight percent of secondary minerals.

APPENDIX B. DATABASE

ID	Litho Group	Lithology	Alt%	Smec vol	Qv dim	k_gas	k_wat	\rho_g	\sigma$_{LS}$	\sigma$_{HS}$	FF
	Group	*Description*	*%*	*%*	-	*mDa*	*mDa*	*g/cm³*	*S/m*	*S/m*	-
L2	Hyalo	welded breccia	58%	12%	0.3	3.0E-01	2.5E-02	2.7E+00	2.2E-02	4.6E-01	25
L5a	Lava	pyroclastic flow	12%	8%	0.4	NaN	NaN	2.7E+00	5.0E-03	1.0E-01	113
L5b	Lava	pyroclastic flow	12%	9%	1.3	5.5E-04	NaN	2.7E+00	2.1E-03	2.7E-02	474
L6	Hyalo	welded breccia	57%	30%	1.1	1.4E-01	7.6E-04	2.6E+00	1.7E-02	1.8E-01	75
L9	Hyalo	Hyaloclastite/Tuff	53%	36%	1.3	NaN	NaN	2.8E+00	3.1E-02	1.9E-01	89
L10	Lava	Vesicular basalt	27%	23%	0.8	NaN	NaN	2.9E+00	1.3E-02	2.0E-01	71
L11	Lava	Crystalline basalt	31%	25%	1.1	3.7E-02	9.0E-04	2.9E+00	1.5E-02	9.3E-02	186
L12a	Lava	pyroclastic flow	6%	7%	1.8	NaN	NaN	3.0E+00	1.2E-03	1.6E-02	1005
L12b	Lava	pyroclastic flow	6%	7%	1.5	1.3E-04	NaN	3.1E+00	1.5E-03	2.5E-02	527
L14	Hyalo	Hyaloclastite/Tuff	67%	28%	0.7	9.3E+00	2.6E-01	2.7E+00	4.1E-02	5.2E-01	19
L15	Lava	Crystalline basalt	20%	22%	2.0	NaN	NaN	2.9E+00	7.7E-03	6.0E-02	267
L16	Lava	Crystalline basalt	25%	25%	2.5	1.1E-02	1.5E-05	2.8E+00	9.8E-03	5.7E-02	293
L19	Lava	Crystalline basalt	28%	23%	1.0	2.4E-02	3.2E-03	2.9E+00	9.5E-03	1.1E-01	122
L21	Lava	Crystalline basalt	29%	30%	2.0	3.6E-02	9.4E-05	2.9E+00	1.1E-02	7.8E-02	211
L22	Lava	Vesicular basalt	32%	28%	2.0	1.9E-02	8.0E-04	2.8E+00	3.8E-02	1.2E-01	207
L24a	Hyalo	Basaltic breccia	38%	30%	1.4	NaN	NaN	2.8E+00	4.0E-02	2.1E-01	88
L24b	Hyalo	Basaltic breccia	38%	32%	1.8	NaN	NaN	2.8E+00	3.5E-02	1.4E-01	163

L25	Hyalo	Basaltic breccia	44%	12%	0.4	2.0E-02	7.0E-03	2.8E+00	5.1E-02	3.9E-01	37
L26	Lava	Crystalline basalt	16%	18%	1.8	NaN	NaN	2.9E+00	6.7E-03	7.3E-02	200
L28	Lava	Crystalline basalt	40%	41%	2.9	NaN	NaN	2.8E+00	5.9E-03	2.7E-02	740
L29	Lava	Vesicular basalt	18%	18%	1.0	NaN	NaN	2.8E+00	7.9E-03	1.1E-01	124
L30	Lava	Crystalline basalt	13%	15%	3.0	NaN	NaN	2.9E+00	3.1E-03	1.7E-02	1125
L31	Hyalo	Hyaloclastite/Tuff	40%	34%	1.4	1.5E-01	4.5E-04	2.8E+00	2.7E-02	2.1E-01	78
L116	Lava	unaltered lava	15%	12%	1.1	NaN	1.0E-07	2.9E+00	3.7E-03	4.3E-02	321
L117	Lava	unaltered lava	8%	9%	1.9	NaN	1.0E-07	2.9E+00	3.0E-03	1.1E-02	NaN
L118	Lava	unaltered lava	8%	9%	1.9	NaN	1.0E-07	2.9E+00	2.9E-03	2.3E-02	716
L119	Hyalo	hyaloclastite	96%	51%	1.9	3.4E-01	2.0E-04	2.6E+00	NaN	1.9E-01	84
L120	Hyalo	hyaloclastite	59%	12%	0.3	7.8E-02	3.8E-03	2.8E+00	2.0E-02	3.4E-01	33
L121	Hyalo	hyaloclastite	52%	25%	0.6	9.2E-01	6.5E-04	2.7E+00	4.1E-02	4.0E-01	31
L122	Hyalo	hyaloclastite	51%	21%	0.5	NaN	2.2E-02	2.8E+00	3.5E-02	5.0E-01	23
L123	Hyalo	hyaloclastite	48%	30%	0.8	2.9E+00	2.1E-02	2.7E+00	1.1E-01	5.1E-01	30
L35	Hyalo	Breccia	24%	24%	2.0	4.4E-01	7.4E-04	2.6E+00	8.2E-03	7.0E-02	236
L36	Lava	Vesicular lava	22%	4%	0.3	1.9E-03	2.4E-03	2.8E+00	1.0E-03	7.7E-02	146
L37	Lava	Vesicular lava	21%	6%	0.2	2.3E-02	7.0E-03	2.8E+00	4.6E-03	2.6E-01	42
L40	Lava	Vesicular lava	28%	11%	0.5	1.5E-03	3.4E-04	2.8E+00	5.8E-03	1.1E-01	121
L41	Hyalo	Basaltic breccia	10%	5%	0.5	NaN	NaN	2.8E+00	3.4E-03	9.6E-02	122
L42	Hyalo	Hyaloclastite/Tuff	11%	6%	0.2	NaN	NaN	2.7E+00	5.9E-03	2.9E-01	39
L43	Lava	Vesicular basalt	13%	1%	0.0	NaN	NaN	3.0E+00	1.3E-03	1.6E-01	64
L44	Lava	Vesicular basalt	11%	1%	0.1	NaN	NaN	3.0E+00	2.2E-03	1.9E-01	53
L45	Lava	Vesicular basalt	12%	1%	0.0	NaN	NaN	2.9E+00	3.8E-03	3.9E-01	25
L46a	Lava	Vesicular basalt	15%	0%	0.0	7.1E-01	5.0E-01	3.0E+00	2.4E-03	3.6E-01	28
L46b	Lava	Vesicular basalt	15%	0%	0.0	NaN	NaN	3.0E+00	2.3E-03	3.6E-01	26
L47	Lava	Vesicular basalt	11%	0%	0.0	NaN	NaN	3.0E+00	3.4E-03	3.4E-01	30
L48	Lava	Vesicular basalt	7%	0%	0.0	NaN	NaN	3.0E+00	2.0E-03	2.4E-01	43
L49	Lava	Vesicular basalt	11%	0%	0.0	NaN	NaN	3.0E+00	6.6E-04	7.0E-02	136
L50	Lava	Crystalline lava	12%	0%	0.0	3.0E-01	1.6E-01	3.0E+00	1.9E-03	2.6E-01	38
L51	Lava	Vesicular basalt	24%	1%	0.0	NaN	NaN	3.0E+00	2.9E-03	3.1E-01	34
L52	Hyalo	Hyaloclastite/Tuff	35%	6%	0.4	NaN	NaN	2.8E+00	3.8E-03	9.4E-02	133
L54	Hyalo	Hyaloclastite/Tuff	23%	2%	0.1	NaN	NaN	2.8E+00	9.1E-04	9.7E-02	109
L55	Hyalo	Basaltic breccia	11%	2%	0.2	1.7E-02	1.0E-02	2.8E+00	2.2E-03	1.4E-01	75
L56	Hyalo	Hyaloclastite/Tuff	16%	2%	0.1	NaN	NaN	2.7E+00	4.8E-03	3.8E-01	27
L57	Hyalo	Hyaloclastite/Tuff	19%	1%	0.0	1.5E+00	7.0E-01	2.9E+00	5.9E-03	5.3E-01	17
L58	Lava	Crystalline basalt	25%	4%	0.3	NaN	NaN	3.0E+00	9.1E-04	3.6E-02	326
L59	Hyalo	Hyaloclastite/Tuff	26%	4%	0.2	NaN	NaN	2.8E+00	3.6E-03	1.7E-01	63
L60	Lava	Lava	29%	8%	0.4	NaN	NaN	2.9E+00	2.0E-03	7.6E-02	162
L61	Hyalo	Basaltic breccia	33%	3%	0.1	NaN	NaN	2.9E+00	4.0E-03	6.6E-01	14
L69	Hyalo	Hyaloclastite/Tuff	13%	2%	0.1	1.5E-01	1.1E-01	2.9E+00	6.5E-03	6.3E-01	14
L71	Hyalo	Hyaloclastite/Tuff	35%	5%	0.1	6.2E-03	5.8E-03	2.9E+00	6.3E-03	4.5E-01	22
L62	Hyalo	Basaltic breccia	16%	1%	0.1	NaN	NaN	2.9E+00	7.8E-04	8.9E-02	116
L73	Hyalo	Basaltic breccia	26%	2%	0.1	NaN	NaN	3.0E+00	2.2E-03	2.6E-01	40
L66	Hyalo	Basaltic breccia	16%	1%	0.1	NaN	NaN	2.9E+00	7.6E-04	9.1E-02	116
L67a	Lava	Vesicular basalt	20%	0%	0.0	NaN	NaN	2.8E+00	1.3E-03	1.9E-01	53
L67b	Lava	Vesicular basalt	20%	0%	0.0	1.4E-01	8.0E-02	2.8E+00	1.7E-03	2.7E-01	38

L75	Lava	Vesicular basalt	8%	1%	0.0	NaN	NaN	2.9E+00	6.2E-04	8.3E-02	117
L76	Lava	Vesicular basalt	22%	2%	0.2	NaN	NaN	3.0E+00	4.5E-04	4.9E-02	243
L106	Lava	unaltered lava	1%	1%	0.7	1.1E-05	NaN	3.0E+00	2.6E-04	1.3E-02	578
L107	Hyalo	hyaloclastite	66%	18%	0.5	2.8E-01	1.2E-03	2.8E+00	4.7E-02	5.1E-01	23
L108	Lava	basaltic lava	15%	13%	2.2	3.6E-04	NaN	2.9E+00	1.6E-03	1.9E-02	521
L109	Lava	basaltic lava	12%	10%	2.5	1.6E-03	NaN	2.9E+00	9.4E-04	2.4E-02	411
L110	Lava	basaltic lava	45%	11%	0.7	4.4E-02	1.3E-04	2.8E+00	2.7E-02	1.7E-01	88
L111	Lava	basaltic lava	28%	9%	1.8	1.2E-03	8.9E-07	2.8E+00	2.8E-03	1.7E-02	693
L112	Lava	doleritic dyke	24%	8%	2.1	7.2E-05	NaN	2.9E+00	1.1E-03	1.4E-02	803
L113	Lava	doleritic dyke	28%	5%	0.5	4.8E-04	2.6E-06	2.9E+00	1.4E-03	3.0E-02	378
L114	Lava	doleritic dyke	20%	3%	0.5	6.3E-04	3.7E-06	2.9E+00	9.1E-04	2.6E-02	445
L115	Lava	very altered lava	36%	7%	0.5	1.2E-03	1.8E-04	2.8E+00	4.6E-03	6.7E-02	178
L81	Lava	Crystalline basalt	23%	27%	3.4	3.5E-03	1.0E-06	2.9E+00	4.7E-03	3.5E-02	461
L82	Lava	very altered lava	24%	5%	0.2	7.0E-03	6.6E-03	2.9E+00	7.4E-03	4.4E-01	22
L85	Lava	Crystalline basalt	10%	5%	1.8	3.9E-04	1.9E-06	2.9E+00	1.2E-03	2.0E-02	683
L87	Lava	very altered lava	14%	6%	0.3	6.2E-03	NaN	2.9E+00	1.8E-03	1.0E-01	119
L91	Hyalo	hyaloclastite	13%	10%	0.9	1.5E-02	8.0E-04	2.9E+00	1.1E-03	2.7E-02	462
L93	Lava	hornfel	8%	2%	0.1	2.5E-02	1.7E-02	2.8E+00	3.0E-03	2.4E-01	42
L96	Hyalo	Basaltic breccia	42%	30%	1.1	2.0E-02	6.0E-04	2.7E+00	3.2E-02	2.7E-01	53
L99	Hyalo	Basaltic breccia	77%	30%	1.0	5.2E-02	5.6E-03	2.7E+00	2.0E-02	3.7E-01	34
L100	Hyalo	Basaltic breccia	36%	33%	1.3	3.9E-02	9.4E-04	2.8E+00	2.9E-02	8.8E-02	147
L102	Hyalo	Hyaloclastite/Tuff	33%	10%	0.4	7.6E-02	1.9E-02	2.7E+00	9.1E-03	3.0E-01	39
L103	Lava	Vesicular basalt	19%	7%	0.4	2.0E-03	NaN	3.0E+00	1.4E-03	6.0E-02	187
L104	Lava	intrusion	26%	28%	2.4	1.7E-04	NaN	3.0E+00	4.6E-03	1.7E-02	1194
L105	Hyalo	hyaloclastite	39%	27%	1.3	8.8E-02	8.5E-04	2.8E+00	2.2E-02	1.9E-01	66
L80	Lava	poorly altered lava	16%	6%	0.5	1.9E-01	2.7E-02	2.9E+00	2.0E-03	NaN	36
L86	Lava	very altered lava	15%	8%	1.2	4.4E-02	1.7E-03	2.9E+00	2.2E-03	NaN	72
L89	Lava	altered lava	17%	6%	0.5	2.9E-04	8.6E-05	2.9E+00	1.2E-03	NaN	150
L95	Hyalo	hyaloclastite	60%	31%	1.3	2.4E-01	6.0E-04	2.7E+00	2.9E-02	NaN	92
L97	Hyalo	hyaloclastite	28%	20%	0.8	4.1E-02	9.0E-04	2.6E+00	2.7E-02	NaN	83
L77	Lava	very altered lava	26%	20%	1.3	5.8E-01	NaN	2.3E+00	NaN	NaN	NaN